Available online at www.sciencedirect.com

ScienceDirect

Procedia IUTAM 14 (2015) 570 – 579

Procedia IUTAM

www.elsevier.com/locate/procedia

IUTAM_ABCM Symposium on Laminar Turbulent Transition

Laminar-turbulent transition in a laminar separation bubble in the presence of free-stream turbulence

Shirzad Hosseinverdi[a,] *, Hermann F. Fasel[a]

[a]*Department of Aerospace and Mechanical Engineering, University of Arizona, Tucson, AZ 85721*

Abstract

Direct numerical simulations (DNS) are employed to investigate the hydrodynamic instability mechanisms and transition to turbulence in laminar separation bubbles (LSBs) on a flat plate. A set of numerical simulations has been carried out to investigate the transition process, and in particular to shed light on the development of the large coherent structures, which arise during transition. Particular focus is directed towards understanding and identifying the relevant physical mechanisms governing the interaction of separation and transition in laminar separation bubbles in the presence of free-stream turbulence (FST). For the natural flow. i.e. zero FST, the transition mechanism involves a Kelvin-Helmholtz instability and a growth of three-dimensional very low-frequency disturbances of the shear layer. With the inclusion of FST, transition is accelerated. For the separation bubbles investigated, the transition process is the result of two different mechanisms: i) Strong amplification of high-frequency (order of the shedding frequency), essentially two-dimensional or weakly oblique fluctuating disturbances and ii) low-frequency, three-dimensional Klebanoff perturbations caused by FST. Depending on the intensity of the FST, one of these mechanisms would dominate the transition process, or both mechanisms are blended together and contribute simultaneously.

Selection and peer-review under responsibility of ABCM (Brazilian Society of Mechanical Sciences and Engineering)

Keywords: Hydrodynamic instability; laminar separation; transition; free-stream turbulence

1. Introduction

A well-founded understanding of the physics of laminar-to-turbulent transition in laminar separation bubbles (LSBs) is key for reliable prediction of the behavior of LSBs in technical applications. Despite considerable advances in the understanding of the relevant mechanisms, a complete understanding of this phenomenon is still missing. Laminar

* Corresponding author. Tel.: +1-520-275-7453.
E-mail address: shirzadh@email.arizona.edu

Selection and peer-review under responsibility of ABCM (Brazilian Society of Mechanical Sciences and Engineering)
doi:10.1016/j.piutam.2015.03.066

separation bubbles are encountered in many practical applications such as low-pressure turbines blades, wings of small unmanned aerial vehicles (UAVs) and rotor blades of wind turbines to name a few.

For a low amplitude-disturbance environment, beyond a certain Reynolds number, Re_{cr}, transition can be initiated by the exponential amplification of so-called Tollmien-Schlichting (TS) waves. Adverse pressure gradients have a destabilizing effect and lower the critical Reynolds number. The presence of an inflection point in the velocity profiles in LSBs gives rise to an inviscid Kelvin-Helmholtz (K-H) instability mechanism. The growth rates associated with the K-H instability are typically much higher than the growth rates associated with TS instabilities for an attached boundary layer. In separated shear layers, two-dimensional disturbances are generally more strongly amplified than 3D disturbances. Therefore, these waves can rapidly reach large (non-linear) amplitudes within the separated region, leading to the commonly observed periodic shedding of spanwise coherent (2D) vortical structures. At this stage, secondary instabilities can take hold, which will subsequently lead to a rapid breakdown to small-scale 3-D structures and eventually to a fully turbulent flow. While the separated regions allow for a rapid growth of vortical disturbances, at the same time the presence of the large-amplitude waves (or vortices) facilitates an exchange of momentum, which limits the extent and intensity of the separation. From the discussion above, it is obvious that separation and transition are intricately linked.

Referred to the above discussion, a number of detailed investigations (theory, experiments and numerical simulations) have addressed laminar-turbulent transition aimed at providing insight into the instability mechanisms in laminar separation bubbles (see Gaster[1]; Watmuff[2]; Diwan & Ramesh[3]; Alam & Sandham[4]; Spalart & Strelets[5]; Rist & Maucher[6]; Postl & Fasel[7]; Hosseinverdi & Fasel[8]; Marxen et al.[9,10]). In those investigations, usually small two-dimensional and/or oblique disturbance waves with a simple spectrum were introduced upstream of the separation and the evolution of the disturbances was tracked all the way to the reattachment region and beyond into the fully turbulent region in order to identify the dominant mechanisms in the separated flow.

The major deficiency of the above transition investigations is that they only address only so-called “controlled transition scenarios” which can only be observed in carefully controlled water/wind tunnel experiments where the environmental disturbances, such as free-stream turbulence (FST), noise and vibrations have been reduced to a minimum. Therefore the question arises whether this path to turbulence is still prevalent in a “real” environment as encountered in free flight, for example. Free-stream turbulence is of particular relevance for technical applications. Atmospheric turbulence is characterized by large length scales and can reach significant turbulent kinetic-energy levels and thus has to be considered when investigating transition in laminar separation bubbles.

For attached boundary layers under natural conditions (e.g., wind tunnels with FST levels Tu>0.1%) transition appears to be preceded by streamwise streaks in the boundary layer. These streaks are now commonly accepted to be caused by ‘Klebanoff-modes’ (or K-modes), after P. S. Klebanoff who first observed them (Klebanoff & Tidstrom[11]; Klebanoff[12]). His findings have been confirmed in numerous experiments by other researchers (Kendall[13]; Westin et al. [14]; Fasel[15]). The streamwise streaks appear to be caused by free-stream turbulence. They have a large downstream extent and a characteristic spanwise length scale of a few boundary-layer thicknesses, δ, of the unperturbed boundary layer. They are fundamentally different both from TS-waves and from the structures commonly observed in turbulent boundary layers. Other characteristic features of the K-modes are their low frequencies and high amplitudes.

The existence of low-frequency, large-amplitude streaks was reported by Häggmark[16] in experiments of laminar separated boundary layers. Free-stream turbulence with an intensity of 1.5% was generated by a grid upstream of the leading edge of the plate. Smoke visualization photographs showed the existence of streaky structures in the boundary layer upstream of the separation and in the separated boundary layer associated with the bubble. No strong evidence for the existence of two-dimensional waves, which are typical for separation bubbles in an undisturbed environment, could be produced. Using spectral analysis, it was shown that lower frequencies are dominant in the case of high FST.

The effect of free-stream turbulence (FST) on laminar separation was investigated by Balzer & Fasel[17]. They carried out a set of DNS based on Gaster’s case VI, series I experiment (Gaster[1]). The free-stream turbulence was introduced at the inflow. They showed that even very small FST levels caused a significant reduction of the size of the separation bubble. Elevated FST levels led to the generation of streamwise boundary-layer streaks, which enhanced the three-dimensional disturbance level. They found that the inviscid shear-layer instability was present for all cases. They showed that transition to turbulence was a consequence of both the primary shear-layer instability and the streamwise streaks caused by the FST.

The main goal of the present work is to contribute towards a better understanding of the highly complex flow physics of laminar separation bubbles subjected to free-stream turbulence. Towards this end, highly-resolved 3D DNS are carried for a LSB developing on a flat plate in the presence of a free-stream pressure gradient, which is the same

as in accompanying water-tunnel experiments, which are carried out in the Hydrodynamics Laboratory at the University of Arizona (see Jagadeesh & Fasel[18]). The present work will attempt to provide a fundamental physics-based understanding of how FST affects laminar-to-turbulent transition in separation bubbles.

2. Computational framework

2.1 Governing Equation and Numerical Methods

The conservation of mass (continuity equation), conservation of momentum (Navier-Stokes equations), form the set of governing equations for the incompressible flow. In the present investigation, the vorticity-velocity formulation in which pressure as a dependent variable is eliminated, is used as follow,

$$\frac{\partial\, \boldsymbol{\omega}}{\partial t} = (\,\boldsymbol{\omega}.\nabla)\,\boldsymbol{u} - (\,\boldsymbol{u}.\nabla)\,\boldsymbol{\omega} + \frac{1}{Re}\nabla^2\,\boldsymbol{\omega}\,. \tag{1}$$

The vorticity vector is defined as $\boldsymbol{\omega} = -\nabla \times \boldsymbol{u}$. Using the fact that the both vorticity and velocity vector fields are solenoidal, one obtains a vector Poisson equation for the velocity field,

$$\nabla^2 \boldsymbol{u} = \nabla \times \boldsymbol{\omega}\,. \tag{2}$$

Both the vorticity and the velocity vector field are solenoidal. In the above equations, all quantities are non-dimensionalized by the free-stream velocity, U_∞, a reference length, L_∞, and the kinematic viscosity, ν. The global Reynolds number is defined as $Re = U_\infty L_\infty/\nu$. A three-dimensional Cartesian coordinate system is employed.

The flow field is assumed to be periodic in the spanwise z-direction. Therefore, the flow variables are expanded in Fourier cosine and sine series. Each variable is represented by a total of *2K+1* Fourier modes: The 2D spanwise average (zeroth Fourier mode), *K* symmetric Fourier cosine as well as *K* antisymmetric Fourier sine modes. To avoid aliasing errors, the nonlinear terms are computed in physical space using $K \approx 3K$ spanwise collocation points.

A three-dimensional Cartesian coordinate system is employed. The governing equations are integrated in time with a standard fourth-order-accurate Runge–Kutta scheme. The spatial derivatives in the streamwise (x) and the wall-normal (y) directions are discretized using fourth-order-accurate compact differences. In the spanwise (z) direction, a pseudo-spectral approach is applied. Fast Fourier Transforms (FFTs) are employed to convert each variable from spectral space to physical space and back, so that the nonlinear terms could be computed in physical space. For the calculation of the nonlinear terms, the flow field is transformed from spectral to physical space (and back) before each Runge-Kutta sub-step, which requires a redistributing of the entire three-dimensional arrays among the processors. This extensive inter-processor communication is realized using the message passing interface (MPI). Details of the numerical method, parallelization, program performance, and of numerous validation cases are presented in Meitz & Fasel[19].

2.2 Method for generating FST in the DNS

The methodology adopted here to generate realistic free-stream disturbances at the inflow boundary of the computational domain is similar to that proposed by Jacobs & Durbin[20]. The method is based on an expansion of the disturbance velocity, $\boldsymbol{u}'$, in terms of its Fourier coefficients,

$$\boldsymbol{u}'(x_0, y, z, t) = \sum_{\boldsymbol{k}} \widehat{\boldsymbol{u}}\,(\boldsymbol{k}, t) e^{i\boldsymbol{k}.\boldsymbol{x}}\,, \tag{3}$$

where $\boldsymbol{k}$ is the wavenumber vector with length $k = \sqrt{k_x^2 + k_y^2 + k_z^2}$. In the same manner, the inflow disturbance vorticity field is calculated from the disturbance velocity field as $\boldsymbol{\omega}' = -\nabla \times \boldsymbol{u}'$. The objective is to specify the Fourier coefficients of a disturbance velocity field such that the inlet disturbance flow field satisfies continuity and generates isotropic turbulence in the free-stream and models a specified energy spectrum. By invoking Taylor's hypothesis and ignoring the streamwise decay, the streamwise wavenumber, $k_x x$, in the definition of $\boldsymbol{k}$, can be replaced by -ωt, where ω is the disturbance frequency. The implementation of the spanwise Fourier modes, $e^{ik_z z}$, is straightforward since the

numerical model assumes periodicity of the flow field in z-direction. However in the presence of the plate, the vortical modes have to decay smoothly to zero towards the wall.

As pointed out in Grosch & Salwen[21], a natural choice for the new basis is the use of the modes of the continuous spectrum. In fact, the Orr–Sommerfeld and Squire eigenvalue problem for a parallel flow in a semi-bounded domain is characterized by the discrete and a continuous spectra. The discrete modes decay exponentially with the distance from the wall, while the continuous modes are oscillatory in the free stream and decay to zero inside the boundary layer (Grosch & Salwen[21]). Instead of Fourier modes $\left(\exp(ik_y y)\right)$ in the expansion of the disturbance quantities, Jacobs & Durbin[20] suggested to use eigenmodes from the continuous spectrum of the Orr-Sommerfeld and Squire operators, therefore equation (3) can be reformulated as

$$\boldsymbol{u}'(x_0, y, z, t) = \sum_{\omega} \sum_{k_z} \sum_{k_y} A\,(|k|)\Phi\left(\omega, k_y, k_z\right) e^{ik_z z} e^{-i\omega t}\,. \tag{4}$$

Here, the coefficients $A(|k|)$ determine the contribution of the eigenfunctions to the total turbulent kinetic energy and Φ is a normalized superposition of Orr–Sommerfeld and Squire continuous eigenfunctions. A detailed description of the implementation and validation results are provided in Balzer & Fasel[17].

2.3 Computational domain

The setup for the DNS was guided by water-tunnel experiments that are being carried out at the Hydrodynamics Laboratory at the University of Arizona[18]. In the experiments a laminar separation bubble is generated on a flat plate through the close proximity of a displacement body with a modified NACA 64_3-618 airfoil. Suction is applied in the aft part of the airfoil to prevent flow separation from the airfoil such that flow separation and reattachment occur only on the flat plate. In the simulation model a wall normal velocity distribution is specified at the free-stream boundary such that the same streamwise pressure distribution was created as in the experiment. The computational setup is shown in Fig. 1. In the numerical simulation, the integration domain does not include the leading edge. The streamwise, wall-normal and spanwise coordinates are x, y, and z, respectively. The domain width in the spanwise direction is $L_z = 3$. The Reynolds number based on inflow displacement thickness and streamwise velocity at the inflow boundary, Re_{δ_1} is 161. All the simulations presented in this work are carried out using the same computational grid with approximately 89 million grid points ($1851 \times 240 \times 200$). The grid spacing is uniform in streamwise direction and the points are stretched exponentially away from the wall in wall-normal direction to improve the resolution near the wall. Free-stream turbulence is introduced at the inflow boundary. A Falkner-Skan velocity profile is prescribed at the inflow, which closely matches that of the experiments. At the downstream boundary, a buffer domain as proposed by Meitz & Fasel[19] is employed in order to smoothly dampen out the turbulent fluctuations generated inside the domain.

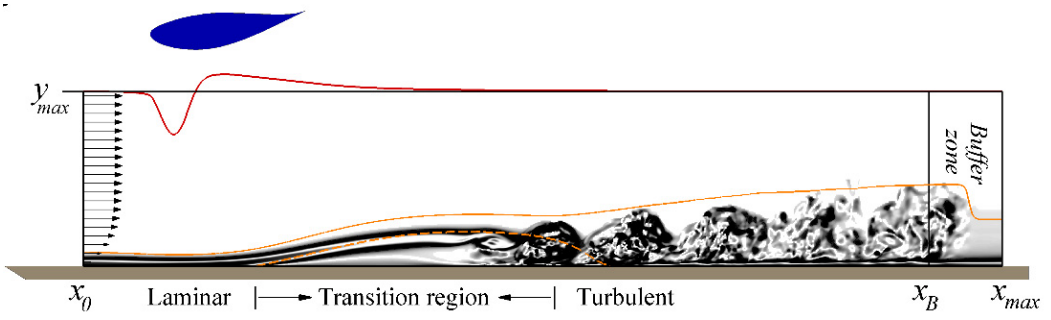

Fig. 1. Schematic illustration of the computational setup. Indicated are the wall-normal velocity distribution at the upper boundary, the velocity profile at the inflow and the buffer zone near the outflow. Also shown are: instantaneous contours of spanwise-averaged ω_z-vorticity, time- and the spanwise-averaged boundary-layer thickness and the dividing streamline (dashed line). The domain extent in the streamwise is $x_0 = 1 \le x \le x_0 = 17.19$, the domain height is $y_{max} = 2$.

3. General characteristic of natural flow simulation, zero FST

In this section results obtained from 3-D DNS are discussed for a case without free-stream turbulence. As mentioned in the introduction, because the velocity profiles in the separated region exhibit an inflection point, the separated shear layer is highly unstable with respect to small disturbances within the flow thus allowing for rapid growth of spanwise vortical structures that can persist even in the turbulent flow region downstream of the reattachment location (coherent structures). To gain insight into the nature of the vortical structures and their evolution, contours of total vorticity in different streamwise stations were analyzed in Fig. 2. The top-left plot shows contours of the streamwise vorticity component at $x = 7$. Starting from left in Fig. 2, the boundary layer separates at $x_s = 4.26$, followed by a very smooth separated shear layer, which has negligible dependency in spanwise direction. Just downstream of the separation location, the vortical structures are mainly confined to the inner region of the boundary layer. Farther downstream, the vortices are lifted into the shear layer. Near $x = 7$, three-dimensionality appears to play a role and two "legs" are extended toward the wall at two different spanwise positions. The spanwise wavelength of the legs is $\lambda_z \approx L_z/2$. Further downstream, the "legs" touch the wall and start to fill out the boundary layer in spanwise direction. Looking at the streamwise vorticity component at $x = 7$ (top-left plot) demonstrates that the "legs" are contour-rotating vortices. Contours of spanwise vorticity reveal that the shear layer undergoes transition, followed by shedding of strong coherent (clockwise-rotating) vortices (often referred to as "rollers"), and finally leading to turbulent reattachment. Downstream of reattachment, the vortices are stretched in wall-normal direction as they are traveling downstream. Near reattachment, the large-scale vortices have penetrated the boundary layer. The vortices maintain coherence in spanwise direction at first while further downstream the spanwise coherence is destroyed. To gain more information into the vortical flow structures, ios-surfaces of the λ_2-criterion by Jeong & Hussain[22] are also shown in Fig. 2. The λ_2-criterion indicates areas where rotation dominates strain. Focus here is on the transitional region where small vortices are concentrated in areas with strong spanwise coherent rollers. The spanwise oriented structures are visible near $x = 9$ before the flow breaks down to smaller scales. Earlier research by Postl et al.[23] suggests that these structures are resulting from a saturation of the 2-D disturbances associated with the primary (Kelvin-Helmholtz) instability of the 2-D mean flow profile. It can be seen that the small-scales are organized in lumps (coherent structures). More important is that the dominant coherent structures persist even downstream of reattachment.

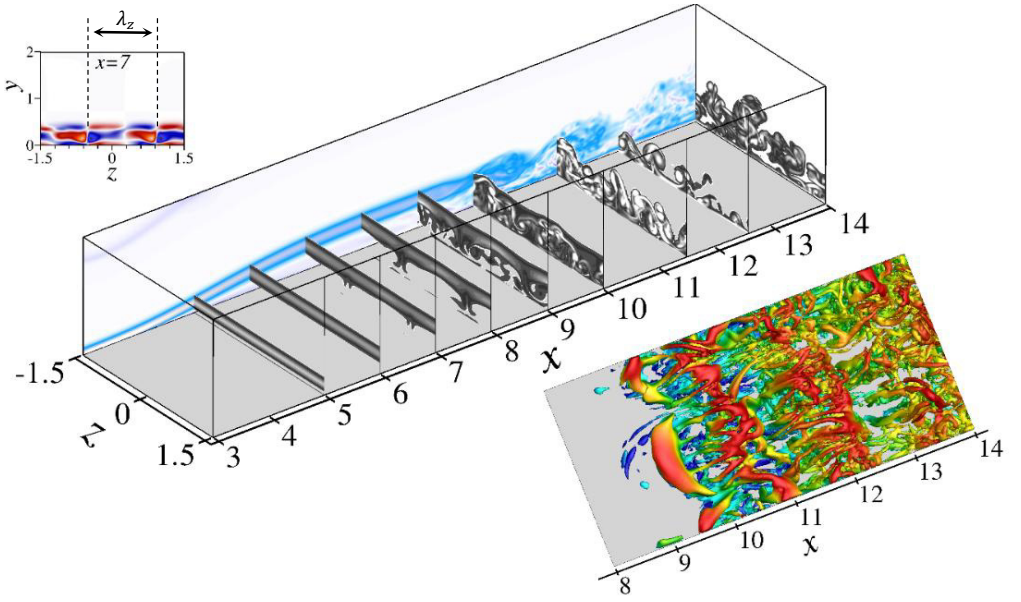

Fig. 2. Visualization of the total vorticity in selected planes for case without FST. Top-left: Contours of streamwise vorticity at x=7; right-bottom: Iso-surfaces of $\lambda_2 = -1$. Also, contours of spanwise vorticity (averaged in spanwise direction) are shown in plane $z = -1.5$.

The time trace of the wall–normal disturbance velocity (averaged in spanwise direction) provide further information of the unsteady nature of the LSB as presented in Fig. 3 for several streamwise locations within the bubble and downstream of reattachment at a fixed distance of 0.42 from the wall (close to the center of shedding vortex core). Frequency spectra associated with these velocity signals are given in Fig. 4. Here, the dimensional frequency is non-dimensionalized as follows:

$$F = \frac{2\pi f^* \nu}{U_\infty^2} 10^6. \qquad (5)$$

Downstream of the separation point at $x = 8.59$, the signal is composed of short (wave-packet like) pulses around $t = 235(s)$ with quite undisturbed steady flow after and before that. The corresponding frequency content (Fig. 4) shows a fairly high level of energy at very low-frequency (f_0). The low frequency content in the spectra may correspond to a so-called "flapping" of the LSB (see Spalart & Strelets[5]). The flapping is related to a long-wave length, vertical oscillation of the separated layer and it usually occurred when no external disturbances were introduced. The signal also exhibits a high frequency content, which is caused by the growth of instability waves in the separated region. Farther downstream, patches of disturbances begin to be more frequent and the time signals become more periodic, yet still highly modulated. These periodic variations are associated with the fundamental shedding cycle of the separation bubble. A distinct peak at the fundamental frequency $F \approx 954$ (f_1) develops for all streamwise locations shown here. The peak is associated with the inviscid shear layer instability. The high-frequency oscillations in the shear layer become more dominant further downstream while the low-frequency characteristics become less pronounced. It appears that strong higher harmonics are also generated nonlinearly (f_2).

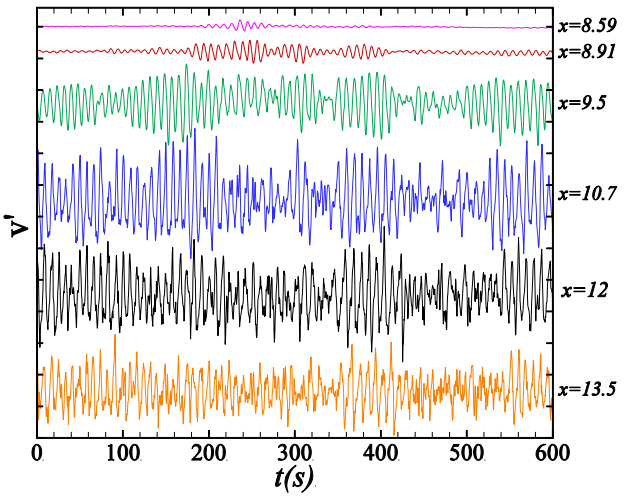

Fig. 3. Temporal and spatial evolution of the wall–normal disturbance velocity (averaged in spanwise direction) at various streamwise locations along the centreline of shear layer.

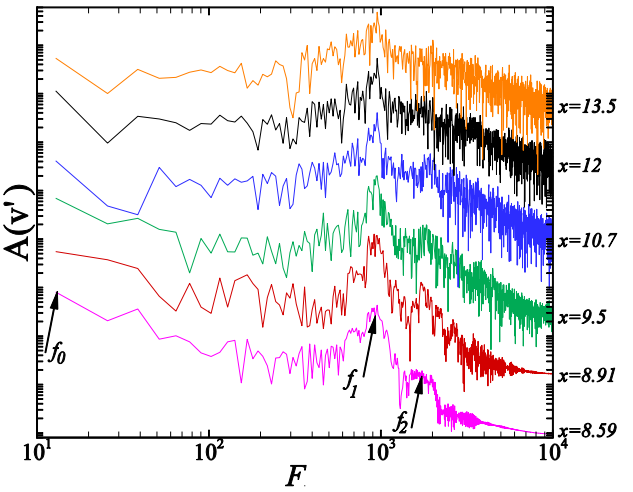

Fig. 4. Frequency spectra for wall–normal disturbance velocity at various streamwise locations along the centreline of the shear layer (see Fig. 3).

4. Effect of free-stream turbulence on transition process

In real technical applications, transition occurs via amplification of naturally occurring background disturbances, such as caused by free-stream turbulence, vibrations or by surface roughness. These disturbances will of course accelerate transition, and as consequence, reduce the size of the separation bubble. Such disturbances are not present in the DNS, except for a low level of background disturbances ('numerical noise'), which can be kept extremely small in our highly resolved simulations using high-order accurate simulation codes. In this section we address laminar-turbulent transition in LSBs exposed to free-stream turbulence in order to explore if and how the FST affects the fundamental flow physics compared to the laminar LSBs without FST. Four different levels of FST were investigated: $Tu = 0.1\%, 0.5\%, 1\%$ and 2%.

The picture changes when isotropic free-stream turbulence is introduced at the inflow boundary as shown in Fig. 5. Transition moves upstream compared to the case without FST when the FST level is increased to $Tu = 0.5\%$.

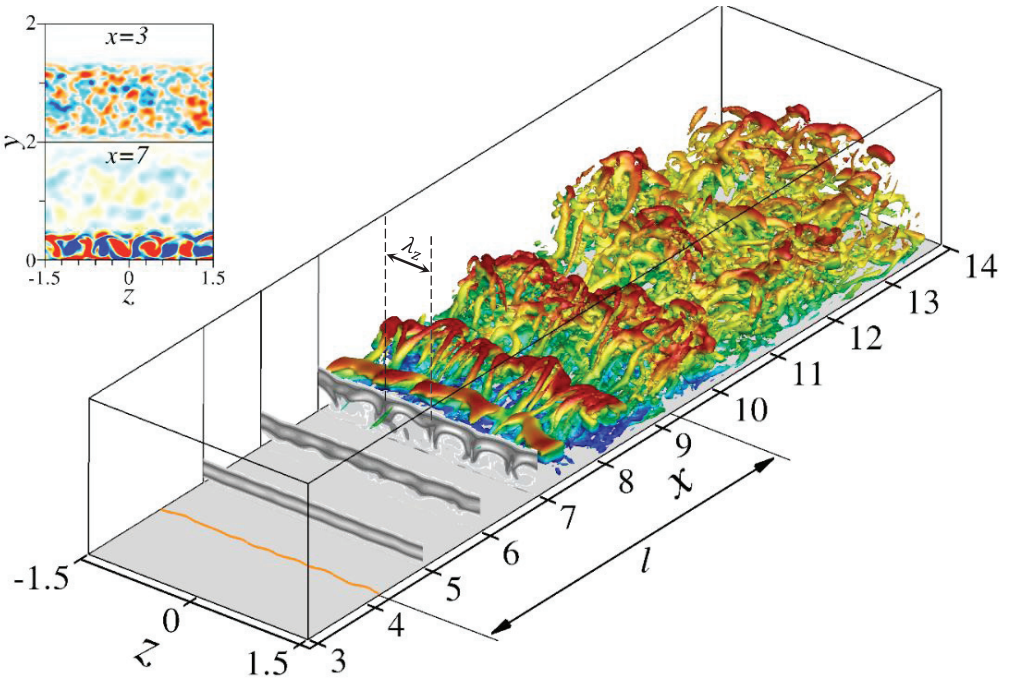

Fig. 5. Iso-surfaces of $\lambda_2 = -1$ together with contours of the total vorticity in selected planes for case with $Tu = 0.5\%$. Top-left: Contours of streamwise vorticity at $x = 3$ & 7. The extent of time- and spanwise-averaged separation length was indicated by l.

Instantaneous iso-surfaces of $\lambda_2 = -1$ are presented in Fig. 5 together with the contours of total vorticity at several streamwise locations. The top-left plots are for the streamwise vorticity at two different planes. The vortical disturbances are present in the free-stream as shown in the left-top plot for $x = 3$. The free-stream vortical disturbances permeate in to the boundary-layer and manifest themselves as the contour-rotating longitudinal vortices (see top-left plot for $x = 7$) with a preferred spanwise wavelength of $\lambda_z = L_z/5$, which can be clearly observed for example at slice x=7 (see perspective view of Fig. 5). These contour-rotating vortices facilitate the exchange of momentum by transporting the low-momentum fluid away the wall and pushing the high-momentum fluid towards the wall. Also one spanwise coherent roller is visible before the flow breaks down to smaller scales.

Spanwise, one-dimensional power spectra of the streamwise velocity component are plotted for selected streamwise locations for $Tu = 1\%$ in Fig. 6. Five x-stations were selected, the inflow boundary, x_{inlet}, the onset of adverse pressure gradient, x_{APG}, the separation location, x_S, the location of maximum bubble height, $x_{h,max}$, and the mean reattachment location, x_R. For the simulations with FST introduced at the inflow, the energy in the power spectrum at the inflow is clearly concentrated in the free-stream and the maximum amplitude is at $1 \leq k \leq 2$, where k is the spanwise mode number (e.g. $k = 1$ indicates that the spanwise width of the disturbances is $\lambda_z = L_z$ and for $k = 2$, $\lambda_z = L_z/2$, where L_z is the domain width in spanwise direction). While propagating in downstream direction, the vortical structures in the free-stream penetrate the boundary layer as can be clearly observed in Fig. 6. At the onset of the pressure gradient, there is preferred spanwise mode number, $k = 5$, for which the disturbances have the maximum amplitude. The disturbances are amplified inside the boundary layer close to the displacement thickness, whereby the spanwise mode $k = 5$ becomes dominant. Close to the location of maximum bubble height, the disturbances have filled the boundary layer, which is more pronounced at the reattachment location where the near-wall peaks appear for a lower spanwise mode number, indicating that the boundary layer is starting to re-develop.

In order to understand the mechanisms responsible for the generation and evolution of the coherent structures, the Fourier decomposed (in time and spanwise direction) flow field was scrutinized in more detail. The wall-normal maxima of the disturbance kinetic energy in the frequency - x plane for 2D modes ($k = 0$) for $Tu = 0.5\%$ and $Tu = 2\%$ are shown in Fig. 7 (top).

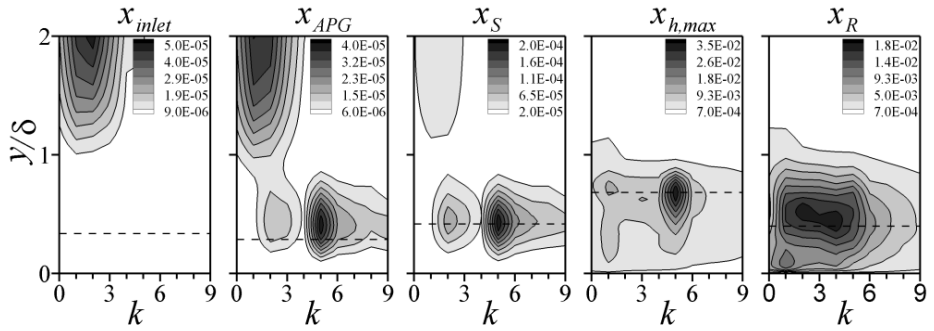

Fig. 6. Spanwise one-dimensional energy spectra of the streamwise velocity at selected streamwise stations for $Tu = 1\%$. Dashed lines are the displacement thickness. Wall-normal coordinates was normalized with the local boundary layer thickness.

A strong peak appears for $F \approx 915$, in the frequency spectra for 2D modes, which corresponds to the fundamental shedding frequency in the bubble. Note that the maximum disturbance kinetic energy decreases as the FST intensity is increased to $Tu = 2\%$. From experiments and numerical simulations (Klebanoff & Tidstrom[11]; Klebanoff[12]; Meitz[24]; Jacobs & Durbin[20]; Fasel[15]), it is known that the FST can cause the formation of streamwise elongated streaks inside the boundary layer, the so-called Klebanoff modes. The Klebanoff mode is a low frequency mode characterized by a distinct spanwise spacing. The spanwise spectra and analysis of the instantaneous flow field obtained from our simulation data provided evidence of a pronounced spanwise periodicity of the stream-wise structures in the laminar and transitional regions. The spanwise spacing and the frequency of the Klebanoff modes can be assessed by evaluating the disturbance kinetic energy spectrum.

From the power spectra in Fig. 6 it is obvious that there is dominant spanwise mode with $k = 5$ for which the disturbances have the maximum amplitude. The wall-normal maximum amplitude of the disturbance kinetic energy in the frequency-x plane at $k = 5$ for cases with $Tu = 0.5\%$ and $Tu = 2\%$ are shown in Fig. 7 (bottom). The shedding frequency, $F = 915$, is shown in the figure by a dashed line. High energy content is observed near $F \approx 26$. The frequency spectra reflect the generation of the low-frequency disturbances, due to the presence of Klebanoff modes, which are amplified in the adverse pressure gradient region. Thus, for the cases with FST, two different modes could be clearly identified: i) The strongly amplified 2D modes with a shedding frequency that is directly related to the Kelvin-Helmholtz instability, and ii) the low-frequency Klebanoff modes. Tracking the downstream development of the disturbance kinetic energy, e, provides additional information regarding the dominant instability mechanisms and a possible shift in importance of the two identified instability modes for different FST intensities. The spectral disturbance kinetic energy for each mode (F, k) was computed from the wall-normal amplitude distributions of the Fourier velocity components,

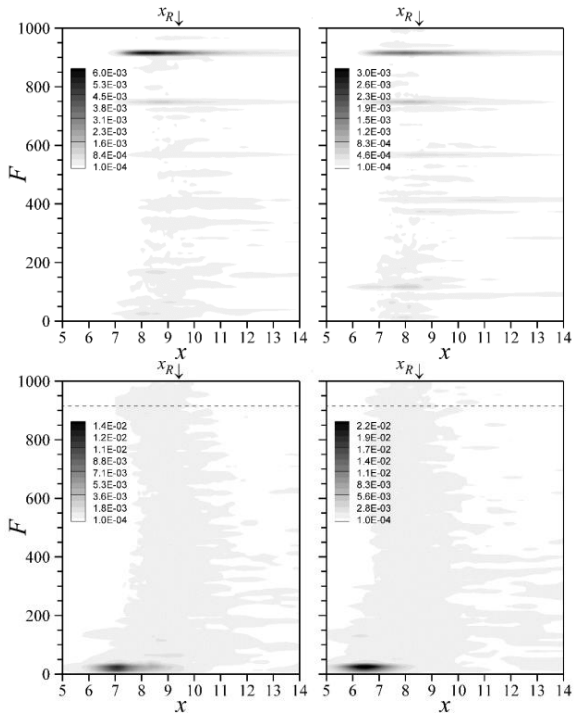

Fig. 7. Disturbance energy spectrum in frequency-x plane for $Tu = 0.5\%$ (left) and $Tu = 2\%$ (right). Plotted are the wall normal maxima inside the boundary-layer. From top to bottom: Two-dimensional modes, $k = 0$; three-dimensional disturbances, $k = 5$. The dashed lines indicate the fundamental shedding frequency. Reattachment is marked by down arrow.

$$e^{(F,k)}(x,y) = \frac{1}{2}\left[u_A^{(F,k)}(x,y)^2 + v_A^{(F,k)}(x,y)^2 + w_A^{(F,k)}(x,y)^2\right]. \quad (6)$$

The notation (F, k) is used for a pair of mode numbers. Here, F is the non-dimensional frequency and $2\pi k/L_Z$ is the spanwise wavenumber of a structure. The maximum amplitude of the Klebanoff modes, $(26, 5)$, are compared with the maximum amplitude of the 2D fundamental modes, $(915, 0)$ for all cases with FST in Fig. 8. For the Klebanoff modes, the streamwise growth is increased for $x > 3.4$ which is the onset of adverse pressure gradient, and the maximum amplitude increases as the free-stream turbulence level is elevated. For the lowest level of FST, $Tu = 0.1\%$, the region upstream of reattachment, which is at the end of the transition region, is dominated by 2D modes, while for the highest FST, $Tu = 2\%$, the Klebanoff modes are dominant in the entire transition region. For the FST levels in between, both modes are blended together and contribute to the transition process simultaneously. One would expect that with increasing FST, the dominant structures would lose their spanwise coherence. Downstream of the mean reattachment location, the K-modes are decaying much faster than the 2D modes.

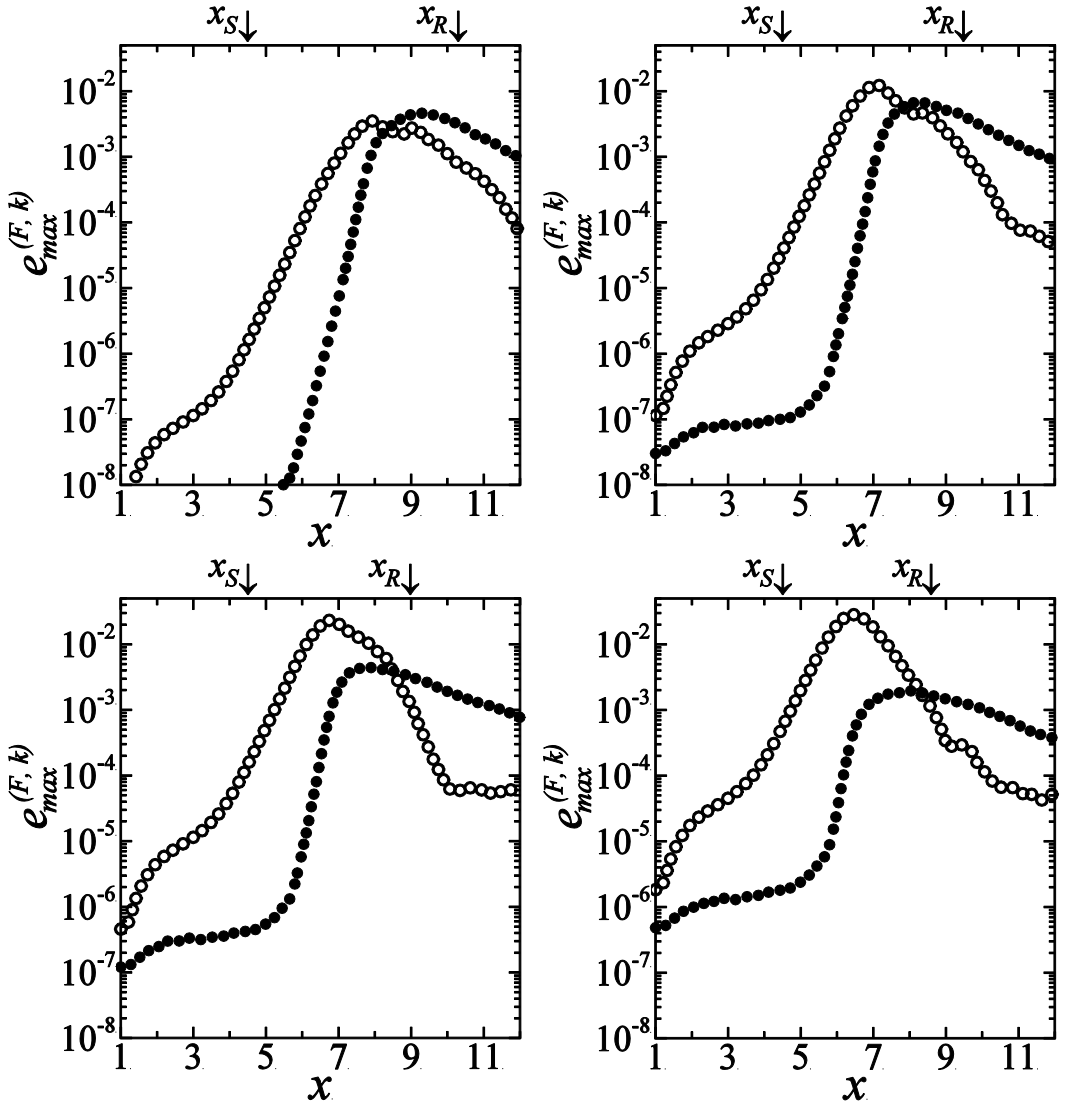

Fig. 8. Comparison of the downstream development between the 2D modes at the fundamental frequency, (915, 0), and the 3D low frequency disturbances, (26, 5). (●) (915, 0); (○) (26, 5). From top-left to bottom-right: $Tu = 0.1\%$; $Tu = 0.5\%$; $Tu = 1\%$; $Tu = 2\%$. Plotted are the wall-normal maxima of the spectral kinetic energy inside the boundary layer. Streamwise locations of separation and reattachment are indicated by down arrows.

5. Conclusion

Highly resolved direct numerical simulations (DNS) were employed to investigate the effect of free-stream turbulence (FST) on transition in laminar separation bubbles on a flat-plate. Towards this end, in the simulations disturbances generated by isotropic free-stream were introduced at the inflow boundary. For modelling of the FST, the continuous modes of the Orr-Sommerfeld and Squire equations were employed. Four different levels of FST intensity, $Tu = 0.1, 0.5, 1.0,$ and 2% were considered. For the simulations with FST, the frequency spectra exhibited a strong peak for two-dimensional modes, which corresponded to the fundamental shedding frequency of the bubbles. Instantaneous flow structures revealed that the vortical disturbances in the free-stream can also generate longitudinal contour-rotating flow structures – the so-called Klebanoff modes (K-modes). Thus, for the cases investigated here, transition to turbulence appeared to be the consequences of the strong amplification of high-frequency disturbances and the low-frequency, three-dimensional disturbances (K-modes). In particular, for the lowest level of FST, $Tu = 0.1\%$, an inviscid Kelvin-Helmholtz (K-H) instability is the dominant mechanism causing transition in the bubble, while for moderate turbulent intensity, $Tu{\sim}0.5 - 1\%$, the disturbances resulting from the K-H instability and the Klebanoff modes caused by FST are blended together and contribute simultaneously to the transition process. For the highest FST intensity, $Tu = 2\%$, the transition mechanism is dominated by K-modes.

Acknowledgements

This work was supported by the Air Force Office of Scientific Research (AFOSR) under grant number FA9550-14-1-0184, with Douglas R. Smith serving as the program manager.

References

1. Gaster M. The structure and behavior of laminar separation bubbles. In *AGARD CP 4* 1969;813–854.
2. Watmuff JH. Evolution of a wave packet into vortex loops in a laminar separation bubble. *J. Fluid Mech* 1999;**397**:119–169.
3. Diwan SS, Ramesh ON. On the origin of the inflectional instability of a laminar separation bubble. *J. Fluid Mech* 2009;**629**:263–298.
4. Alam M, Sandham ND. Direct numerical simulation of 'short' laminar separation bubbles with turbulent reattachment. *J. Fluid Mech* 2000;**403**:223–250.
5. Spalart PR, Strelets MK. Mechanisms of transition and heat transfer in a separation bubble. *J. Fluid Mech* 2000;**403**:329–349.
6. Rist U, Maucher U. Investigations of time-growing instabilities in laminar separation bubbles. *Eur. J. Mech. - B/Fluids* 2002; **21** (5):495–509.
7. Postl D, Fasel HF. Interaction of separation and transition in boundary layers: Direct numerical simulations. In *Laminar-Turbulent Transition, Proceedings of the IUTAM Symposium* 2006; 71–88, India.
8. Hosseinverdi S, Fasel H. Direct Numerical Simulations of Transition to Turbulence in Two-Dimensional Laminar Separation Bubbles. *AIAA Paper* **2013-0264**.
9. Marxen O, Lang M, Rist U, Levin O, Henningson DS. Mechanisms for spatial steady three-dimensional disturbance growth in a non-parallel and separating boundary layer. *J. Fluid Mech* 2009;**634**:165–189.
10. Marxen O, Rist U, Wagner S. The effect of spanwise-modulated disturbances on transition in a 2-D separated boundary layer. *AIAA J* 2004; **42**:937–944.
11. Klebanoff PS, Tidstrom KD. Evolution of amplified waves leading to transition in a boundary layer with zero pressure gradient. NASA 1959;TN D 195.
12. Klebanoff P. Effect of freestream turbulence on the laminar boundary layer. *Bull. Am. Phys. Soc* 1971;**10**:No. 11.
13. Kendall JM. Boundary layer receptivity to freestream turbulence. *AIAA Paper* 1990;**1990-1504.**
14. Westin KJA, Boiko AV, Klingmann BGB, Kozlov VV, Alfredsson PH. Experiments in a boundary layer subjected to freestream turbulence. part 1. boundary layer structure and receptivity. *J Fluid Mech* 1994;**281**:193–218.
15. Fasel HF. Numerical investigation of the interaction of the Klebanoff-mode with a Tollmien-Schlichting wave. *J. Fluid Mech* 2002;**450**:1–33.
16. Häggmark C. Investigations of disturbances developing in a laminar separation bubble flow. *PhD thesis* 2000, KTH, Department of Mechanics, Stockholm.
17. Balzer, W. & Fasel, H. F. Direct numerical simulation of laminar boundary layer separation and separation control on the suction side of an airfoil at low Reynolds number conditions. *AIAA Paper* 2010;**2010-4866**.
18. Jagadeesh CS, Fasel HF. Experimental investigation of the structure and dynamics of laminar separation bubbles. *AIAA paper* 2012;**2012-0755**.
19. Meitz H, Fasel HF. A compact-difference scheme for the Navier-Stokes equations in vorticity-velocity formulation. *J. Comp. Phys* 2000;**157**:371–403.
20. Jacobs RG, Durbin PA. Simulations of Bypass Transition. *J. Fluid Mech* 2001;**421**:185-212.
21. Grosch CE, Salwen H. The continuous spectrum of the Orr-Sommerfeld equation. Part 1. The spectrum and the eigenfunctions," *J. Fluid Mech* 1978;**68**:33–54.
22. Jeong J, Hussain F. On the identification of a vortex. *J. Fluid Mech* 1995;**285**:69–94.
23. Postl D, Balzer W, Fasel H. Control of laminar separation using pulsed vortex generator jets: direct numerical simulations. *J. Fluid Mech* 2011; **676**:81-109.
24. Meitz, H. Numerical investigation of suction in a transitional flat-plate boundary layer. *PhD thesis* 1996, University of Arizona.